

Emergency supplies transportation robot trajectory tracking control based on Koopman and improved event-triggered model predictive control

Yaqi Zhang¹, Minan Tang¹, Haiyan Zhang², Bo An¹, Yaguang Yan¹, Wenjuan Wang¹, and Kunxi Tang¹

¹Lanzhou Jiaotong University

²Jinan New and Old Kinetic Energy Conversion Starting Area Management Committee

April 29, 2023

Abstract

In the emergency rescue and disposal of social public emergencies, supply transportation effectively provides a strong supply foundation and realistic conditions. The trajectory tracking control of emergency supplies transportation robot is the key technology to ensure the timeliness of transportation. In this paper, the emergency supplies transportation robot is taken as the research object, based on Koopman operator theory, combined with radial basis function (RBF) neural network disturbance observer and adaptive prediction horizon event-triggered model predictive control (APET-MPC) algorithm to investigate the purely data-driven trajectory tracking control problem of emergency supplies transportation robot when the model parameters and models are unknown. Firstly, the Koopman operator is used to establish a high-dimensional linear model of the robot. Secondly, the RBF neural network disturbance observer is designed to estimate the disturbance during the robot operation and compensate it to the controller. Thirdly, APET-MPC is used to optimize the trajectory tracking control of the emergency supplies transportation robot to reduce computational complexity. Finally, the performance of the proposed trajectory tracking controller is verified by Carsim/ Simulink joint simulation. The simulation results show that the model established by Koopman operator theory can achieve the high accuracy approximation of the robot. Compared with the MPC trajectory tracking controller, the APET-MPC trajectory tracking controller based on RBF neural network disturbance observer (RBF-APET-MPC) improves the tracking accuracy of the robot and reduces the total triggering times of the system by more than 50%.

ARTICLE TYPE

Emergency supplies transportation robot trajectory tracking control based on Koopman and improved event-triggered model predictive control

Yaqi Zhang¹ | Minan Tang*^{1,3} | Haiyan Zhang² | Bo An¹ | Yaguang Yan¹ | Wenjuan Wang³ | Kunxi Tang¹

¹School of Automation and Electrical Engineering, Lanzhou Jiaotong University, Lanzhou, China

²Construction Management Department, Jinan New and Old Kinetic Energy Conversion Starting Area Management Committee, Jinan, China

³School of New Energy and Power Engineering, Lanzhou Jiaotong University, Lanzhou, China

Correspondence

*Minan Tang, School of Automation and Electrical Engineering, Lanzhou Jiaotong University, Lanzhou, Gansu 730070, China.
Email: tangminan@mail.lzjtu.cn

Summary

In the emergency rescue and disposal of social public emergencies, supply transportation effectively provides a strong supply foundation and realistic conditions. The trajectory tracking control of emergency supplies transportation robot is the key technology to ensure the timeliness of transportation. In this paper, the emergency supplies transportation robot is taken as the research object, based on Koopman operator theory, combined with radial basis function (RBF) neural network disturbance observer and adaptive prediction horizon event-triggered model predictive control (APET-MPC) algorithm to investigate the purely data-driven trajectory tracking control problem of emergency supplies transportation robot when the model parameters and models are unknown. Firstly, the Koopman operator is used to establish a high-dimensional linear model of the robot. Secondly, the RBF neural network disturbance observer is designed to estimate the disturbance during the robot operation and compensate it to the controller. Thirdly, APET-MPC is used to optimize the trajectory tracking control of the emergency supplies transportation robot to reduce computational complexity. Finally, the performance of the proposed trajectory tracking controller is verified by Carsim/ Simulink joint simulation. The simulation results show that the model established by Koopman operator theory can achieve the high accuracy approximation of the robot. Compared with the MPC trajectory tracking controller, the APET-MPC trajectory tracking controller based on RBF neural network disturbance observer (RBF-APET-MPC) improves the tracking accuracy of the robot and reduces the total triggering times of the system by more than 50%.

KEYWORDS:

Trajectory tracking control, model predictive control, event-triggered mechanism, Koopman operator, neural network disturbance observer

1 | INTRODUCTION

The primary task of emergency management is to reduce casualties and losses in disaster areas through effective emergency rescue operations,¹ and any action of emergency events is inseparable from the guarantee and support of supplies. The smooth

flow of information requires accurate and timely transportation of emergency communication equipment, the role of disaster relief personnel depends on the smooth flow of logistics, and the survival of people in disaster areas needs the timely supply of supplies.² Therefore, the efficient transportation of emergency supplies is a key link in dealing with emergencies.³ Due to the suddenness and unpredictability of emergency events,⁴ carrying out efficient and orderly emergency rescue operations can minimize casualties and property losses.⁵ The flexible emergency supplies transportation robot provides convenience for rescue work. For the randomness and urgency of emergency supplies transportation,^{6,7} higher requirements are put forward for the efficient and accurate transportation behavior of emergency supplies transportation robots to ensure people's livelihood and improve efficiency.

The emergency supplies transportation robot provides convenience for transporting supplies, and as the top priority of emergency rescue work, the core problem of emergency supplies transportation is how to accurately track the pre-set reference trajectory in the shortest time, and deliver the supplies to the designated location in the most stable way, taking into account various factors such as time cost, accuracy and stability to ensure timely delivery of emergency supplies. To improve the robustness of robot trajectory tracking control, domestic and foreign scholars have carried out a lot of research, and different control methods have been applied to trajectory tracking control, such as PID control,^{8,9} adaptive control,^{10,11} sliding mode control,^{12,13,14} neural network control,^{15,16} and so on. Model predictive control (MPC) has the excellent characteristics of easy modeling and effective handling of multivariate and constrained problems.¹⁷ It also has the remarkable characteristics of being able to compensate for the uncertainty caused by model mismatch, disturbance and other factors promptly with better dynamic performance, which is widely used in robot trajectory tracking control in recent years, such as References 18, 19, 20.

The first step in analyzing complex control objects is usually modeling, so obtaining a high-accuracy model of complex systems is important. The system model obtained by mechanism modeling can be more limited in its application due to its weak anti-disturbance ability.²¹ The robot system has high nonlinearity, strong coupling, parameter uncertainty, etc.²² For the control of the nonlinear system, the traditional method is to linearize the model locally,^{23,24} but the computational effort is large. The Koopman theory was proposed by B. O. Koopman in 1931,²⁵ which is a powerful tool for data-driven modeling emerging in recent years. The basic idea is to lift the nonlinear system to a linear infinite dimensional space.²⁶ The Koopman theory can be used to obtain the model of the unknown system from the known data and to globally linearize the nonlinear system.²⁷ Reference 28 to accurately capture the transient process of the power grid, a deep neural network method was used to train observable functions to approximate the Koopman operator, overcoming the challenge of high-dimensional nonlinearity in the power grid. Reference 29 applied Koopman theory to the batch pulping process, combined with the model predictive control framework to regulate the Kappa number and cell wall thickness of fibers. In Reference 30, the Koopman operator was used to capture the inherent characteristics of driver-vehicle system dynamics and generate an explicit control-oriented driver-vehicle model in an infinite-dimensional space. The emergency supplies transportation robot operates in a complex environment and will inevitably be affected by friction and external disturbance during actual operation, so it is necessary to suppress the disturbance to the system. Reference 31 designed a nonlinear disturbance observer with an extended Kalman filter to suppress random noise and observe the speed and non-random disturbance of the mobile robot. Reference 32 used RBF neural network design disturbance observer and adaptive parameter adjustment law to estimate the comprehensive disturbance to the flexible spacecraft in real-time. Reference 33 designed a nonlinear disturbance observer to estimate external disturbance and parameter uncertainty to the quadrotor, which the application was more general because the observer did not assume that the disturbance was constant or its upper bound was known.

The model predictive control needs to solve the optimization problem at each sampling time, which requires a lot of computational effort³⁴ and only the first control variable of the obtained control sequence is applied to the real system,³⁵ which implies a waste of computational resources. The event-triggered mechanism can effectively reduce the frequency of solving the optimization problem. Reference 36 proposed a distributed MPC for unmanned aerial vehicles formation control and proposed an event-triggered mechanism considering the predictive state error and the convergence of the cost function to reduce the computational effort. In Reference 37, a novel distributed control law with an event-triggered communication mechanism was proposed for the coordinated control of a multiagent system with input-constrained, and the number of communications between vehicles was reduced and the communication frequency was reduced by the event-triggered communication mechanism. Reference 38 designed an event-triggered update tracking controller for the unicycle robot, which can reduce the average frequency of solving the optimization problem, and the dimension of OCP is reduced by adaptively reducing the prediction horizon when the tracking error approaches the terminal region.

Based on this, this paper combines Koopman theory, radial basis function (RBF) neural network disturbance observer, and adaptive prediction horizon event-triggered model predictive control (APET-MPC) algorithm to study the trajectory tracking

control problem of the emergency supplies transportation robot. Firstly, a high-dimensional linear model of the emergency supplies transportation robot is established by Koopman theory, which is generated by a data-driven method and can effectively predict the future output of the system. Aiming at the disturbance during the operation of the emergency supplies transportation robot, the RBF neural network disturbance observer is used to estimate and compensate for the disturbance in real-time. An event-triggered model predictive control is designed for the trajectory tracking problem of the disturbed incomplete constrained robot, and an adaptive prediction horizon strategy is introduced to reduce the computational complexity by reducing the frequency of solving the optimization problem and to reduce the dimensionality of the optimization problem by shortening the prediction horizon. The introduction of the event-triggered mechanism greatly reduces the MPC computational load. Finally, the modeling accuracy of the Koopman operator and the effectiveness of the APET-MPC (RBF-APET-MPC) trajectory tracking controller based on the RBF neural network disturbance observer are verified by simulation experiments. The simulation results show that using the Koopman operator can obtain a high-accuracy robot model, the RBF neural network disturbance observer can achieve the approximate estimation of disturbance, and the APET-MPC can reduce the computational load of the controller for real-time optimization while ensuring the trajectory tracking accuracy.

The rest of this paper is organized as follows. Section 2 establishes a Koopman high-dimensional linear model for emergency supplies transport robot. Section 3 uses an RBF neural network disturbance observer to estimate the disturbance of the robot during operation. In Section 4, the APET-MPC trajectory tracking controller is designed. The accuracy of the Koopman linear model and the trajectory tracking control effect are simulated and analyzed in Section 5. The conclusion is given in Section 6.

2 | ROBOT MODELING BASED ON KOOPMAN OPERATOR

2.1 | Koopman operator theory

The emergency supplies transportation robot is regarded as a discrete nonlinear system with external input:

$$\mathbf{x}(k+1) = f(\mathbf{x}(k), \mathbf{u}(k)). \quad (1)$$

where $k \in \mathbb{Z}$ is the discrete time step, $\mathbf{x}(k) \in \mathcal{N} \subseteq \mathbb{R}^n$ is the state variable of the system, and $\mathbf{x}(k) = [x(k) \ y(k) \ \varphi(k)]^T$, $\mathbf{u}(k) \in \mathcal{M} \subseteq \mathbb{R}^m$ is the control input of the system, and $\mathbf{u}(k) = [v(k) \ \delta(k)]^T$, n and m are the dimensions of the system state and input, respectively, \mathcal{N} and \mathcal{M} are the state space, \mathbb{R} is the real number domain, \mathbb{R}^n is the Euclidean space of n -dimensional real-valued vector, x and y are the position information, φ is the yaw angle, v is the running speed and δ is the front wheel angle. $f(\mathbf{x}, \mathbf{u})$ represents the nonlinear kinematics of the system state evolution with time. Figure 1 shows the diagram of the emergency supplies transportation robot.

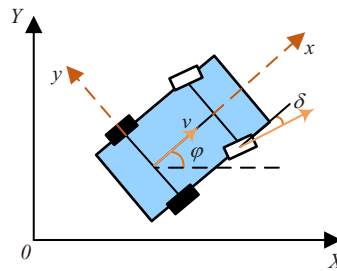


Figure 1 Diagram of emergency supplies transportation robot.

Assumption 1. Assume that $f(0, 0) = 0$ and $f(\mathbf{x}, \mathbf{u}) = 0$ are locally Lipschitz in the domain $\mathcal{N} \times \mathcal{M}$ with Lipschitz constant L_f .

Combine the state variable $\mathbf{x}(k)$ with the control input $\mathbf{u}(k)$ into the extended state:

$$\zeta = \begin{bmatrix} \mathbf{x}(k) \\ \mathbf{u}(k) \end{bmatrix}. \quad (2)$$

The extended system is described by introducing the left shift operator S in the input sequence \mathbf{u} :

$$f_\zeta(\zeta) = \begin{bmatrix} f(\mathbf{x}, \mathbf{u}(0)) \\ S\mathbf{u} \end{bmatrix}. \quad (3)$$

$$S\mathbf{u}(k) = \mathbf{u}(k+1). \quad (4)$$

where f_ζ represents the system kinematics equation of the extended state and $\mathbf{u}(0)$ represents the first element of the control sequence in the current time step.

Define real-valued observation function $\phi: \mathcal{N} \times \mathcal{M} \rightarrow \mathbb{R}$ concerning state and input, which belongs to the infinite-dimensional Hilbert space,³⁹ the Koopman operator \mathcal{K} acts on the real-valued observation function ϕ :

$$\mathcal{K}\phi(\zeta) = \phi(f_\zeta(\zeta)). \quad (5)$$

where $\mathcal{K}: \mathcal{H} \rightarrow \mathcal{H}$ is the Koopman operator for the extended state ζ in (2), and \mathcal{H} is the observable state space of the extended observable function.

Even if the original nonlinear system state is finite-dimensional, \mathcal{K} still maintains the infinite-dimensional characteristics and is linear in \mathcal{H} , i.e.:

$$\mathcal{K}(\alpha\phi_1(\zeta) + \beta\phi_2(\zeta)) = \alpha\mathcal{K}\phi_1(\zeta) + \beta\mathcal{K}\phi_2(\zeta). \quad (6)$$

where $\phi_1, \phi_2 \in \mathcal{F}$ is an arbitrary scalar function on the state space and $\alpha, \beta \in \mathbb{R}$ is an arbitrary constant. By analyzing the infinite-dimensional linear operator \mathcal{K} , the global linearization model of the finite-dimensional nonlinear system can be obtained, as shown in Figure 2.

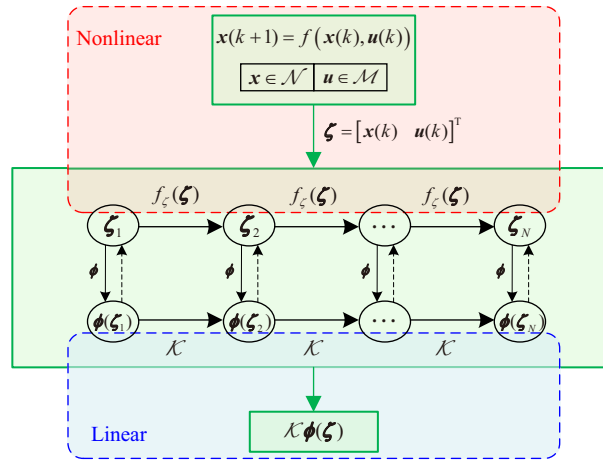


Figure 2 Koopman modeling diagram.

2.2 | Extended dynamic mode decomposition

The linear characteristics of the Koopman operator bring convenience to the application of linear control schemes. However, the infinite-dimensional characteristics of the Koopman operator pose have hindered practical applications. To solve the high-dimensional matrix as an approximation of the Koopman operator, the Extended Dynamic Mode Decomposition (EDMD) algorithm is used to calculate the finite-dimensional projection on the finite-dimensional subspace of all observables.

The Koopman operator is approximated using the dataset generated by the original system,⁴⁰ that is:

$$\zeta_i^+ = f_\zeta(\zeta_i) = \begin{bmatrix} f(\mathbf{x}_i, \mathbf{u}_i(0)) \\ S\mathbf{u}_i \end{bmatrix}. \quad (7)$$

where the superscript + represents the value of the next time step, $i = 1, \dots, N$.

The vector of the extended observable function is:

$$\boldsymbol{\phi}(\zeta) = \begin{bmatrix} \boldsymbol{\psi}(\mathbf{x}) \\ \mathbf{u}(0) \end{bmatrix}. \quad (8)$$

where $\boldsymbol{\psi}(\mathbf{x}) = [\psi_1(\mathbf{x}), \psi_2(\mathbf{x}), \dots, \psi_M(\mathbf{x})]^T$, M is the number of observable functions for the system state $\psi_i(\mathbf{x})$.

The finite-dimensional approximation of the Koopman operator $\tilde{\mathcal{K}}$ is obtained by solving the least squares error problem for the collected dataset by minimizing the following equation:

$$\min_{\tilde{\mathcal{K}}} \sum_{i=1}^N \|\boldsymbol{\phi}(\zeta_i^+) - \tilde{\mathcal{K}}\boldsymbol{\phi}(\zeta_i)\|^2. \quad (9)$$

where $\|\cdot\|$ is the Euclidean norm.

Since there is no need to predict the future control input \mathbf{u}^+ , eliminating the last m elements of the term $\boldsymbol{\phi}(\zeta_i^+)$ and the last m rows of the $\tilde{\mathcal{K}}$ matrix in (9) to obtain $\bar{\mathcal{K}}$.⁴¹ Therefore, the minimization problem (9) can be simplified to:

$$\min_{\bar{\mathcal{K}}} \sum_{i=1}^N \|\boldsymbol{\psi}(\mathbf{x}_i^+) - \bar{\mathcal{K}}\zeta_i\|^2. \quad (10)$$

$\bar{\mathcal{K}}$ can be decomposed into $\bar{\mathcal{K}} = [\mathbf{A} \ \mathbf{B}]$, where both $\mathbf{A} \in \mathbb{R}^{M \times M}$ and $\mathbf{B} \in \mathbb{R}^{M \times m}$ are linear constant matrix, and the minimization problem (10) is transformed into (11):

$$\min_{\mathbf{A}, \mathbf{B}} \sum_{i=1}^N \|\boldsymbol{\psi}(\mathbf{x}_i^+) - \mathbf{A}\boldsymbol{\psi}(\mathbf{x}_i) - \mathbf{B}\mathbf{u}_i(0)\|^2. \quad (11)$$

Finally, by using the matrices \mathbf{A} and \mathbf{B} derived from (11), the linear system of lifting state $\mathbf{z} = \boldsymbol{\psi}(\mathbf{x}) \in \mathbb{R}^M$ with M as the dimension lifted dimension:

$$\mathbf{z}(k+1) = \mathbf{A}\mathbf{z}(k) + \mathbf{B}\mathbf{u}(k). \quad (12)$$

In addition, let the output state:

$$\mathbf{y}(k) = g(\mathbf{x}(k)). \quad (13)$$

Solve the following minimization problem in the least squares sense:

$$\min_{\mathbf{C}} \sum_{i=1}^N \|y_i - \mathbf{C}\boldsymbol{\psi}(\mathbf{x}_i)\|^2. \quad (14)$$

where $\mathbf{C} \in \mathbb{R}^{n \times N}$ is the linear constant matrix. The linear model of \mathbf{y} can be derived from the matrix \mathbf{C} :

$$\mathbf{y}(k) = \mathbf{C}\mathbf{z}(k). \quad (15)$$

2.3 | Numerical approximation of the Koopman operator

Approximate the Koopman operator from the data using an easy-to-implement least squares method. Assuming that the following input and output datasets are collected in the nonlinear dynamic system (1):

$$\mathbf{X} = [\mathbf{x}_1, \dots, \mathbf{x}_k], \mathbf{Y} = [\mathbf{y}_1, \dots, \mathbf{y}_k], \mathbf{U} = [\mathbf{u}_1, \dots, \mathbf{u}_k]. \quad (16)$$

The matrices $\mathbf{X} \in \mathbb{R}^{M \times k}$ and $\mathbf{Y} \in \mathbb{R}^{M \times k}$ contain the observable values of the state. The matrix $\mathbf{U} \in \mathbb{R}^{m \times k}$ contains the input. After obtaining \mathbf{X} , \mathbf{Y} , and \mathbf{U} in (16), the \mathbf{A} , \mathbf{B} , and \mathbf{C} matrices in the high-dimensional model can be obtained by solving the following minimization problem:²⁷

$$\min_{\mathbf{A}, \mathbf{B}} \left\| \mathbf{Y}_{lift} - \mathbf{A} \mathbf{X}_{lift} - \mathbf{B} \mathbf{U} \right\|_2. \quad (17)$$

$$\min_{\mathbf{C}} \left\| \mathbf{X} - \mathbf{C} \mathbf{X}_{lift} \right\|_2. \quad (18)$$

where the symbol $\|\cdot\|_2$ represents 2-norm, $\mathbf{X}_{lift} = [\boldsymbol{\psi}(\mathbf{x}_1) \cdots, \boldsymbol{\psi}(\mathbf{x}_k)]$, $\mathbf{Y}_{lift} = [\boldsymbol{\psi}(\mathbf{y}_1) \cdots, \boldsymbol{\psi}(\mathbf{y}_k)]$.

Using the normal equation⁴² to solve the least squares (17):

$$\mathbf{V} = [\mathbf{A} \ \mathbf{B}] \mathbf{G}. \quad (19)$$

where $\mathbf{G} = \begin{bmatrix} \mathbf{X}_{lift} \\ \mathbf{U} \end{bmatrix} \begin{bmatrix} \mathbf{X}_{lift} \\ \mathbf{U} \end{bmatrix}^T$, $\mathbf{V} = \mathbf{Y}_{lift} \begin{bmatrix} \mathbf{X}_{lift} \\ \mathbf{U} \end{bmatrix}^T$, the matrices \mathbf{A} , \mathbf{B} and \mathbf{C} are obtained as:

$$[\mathbf{A} \ \mathbf{B}] = \mathbf{V} \mathbf{G}^\dagger. \quad (20)$$

$$\mathbf{C} = \mathbf{X} \mathbf{X}_{lift}^\dagger. \quad (21)$$

where \dagger is the Moore–Penrose pseudoinverse.

According to the Koopman operator theory, the linear model of the emergency supplies transportation robot is obtained as follows:

$$\begin{cases} \mathbf{z}(k+1) = \mathbf{A} \mathbf{z}(k) + \mathbf{B} \mathbf{u}(k) \\ \mathbf{y}(k) = \mathbf{C} \mathbf{z}(k) \end{cases}. \quad (22)$$

The (22) is the global linearized model of the nonlinear kinematics system under the action of the Koopman operator. The Koopman high-dimensional model gets rid of the limitations of the original nonlinear system model.

3 | DESIGN OF RBF NEURAL NETWORK DISTURBANCE OBSERVER

Koopman operator can use the offline input and output data of the system to obtain a high-dimensional model of the nonlinear system to predict the robot state. However, the robot itself will inevitably be affected by friction and external disturbance in the actual control process, and the integrated disturbance is difficult to measure accurately. Therefore, the model generated by offline data cannot effectively achieve the state prediction, which will lead to the reduction of control accuracy and even make the system unstable. In the actual system, to obtain a more accurate high-dimensional model of the emergency supplies transportation robot, the disturbance observer is needed to estimate and compensate the disturbance in real-time, and the high-dimensional linear model obtained offline is corrected online to achieve a high-accuracy trajectory tracking effect of the emergency supplies transportation robot.

RBF is a neural network with good local nonlinear approximation, which can approximate any nonlinear function with any accuracy. Therefore, the disturbance observer based on RBF neural network is designed to estimate the disturbance.

The Koopman high-dimensional model of the emergency supplies transportation robot containing disturbance is:

$$\mathbf{y}(k+1) = \mathbf{C} \mathbf{A} \mathbf{z}(k) + \mathbf{C} \mathbf{B} \mathbf{u}(k) + \mathbf{d}(k). \quad (23)$$

where $\mathbf{d}(k)$ is external disturbance. The RBF neural network is used to approximate the disturbance $\mathbf{d}(k)$ in (23) online.

Assumption 2.⁴³ For any $\mathbf{x} \in M_x$, where M_x is a compact set, the optimal weight w_i^* of the RBF neural network approximation disturbance is defined as:

$$w_i^* = \arg \min_{w_i \in \Omega_i} \left[\sup_{x \in M_x} |d_i - \hat{d}_i| \right]. \quad (24)$$

where $\Omega_i = \{w_i \mid \|w_i\| \leq M_w\}$ is the feasible region of the parameter and M_w is the design parameter.

Assumption 3. Given the upper bound of any approximation error $\bar{\epsilon} > 0$, there exists a finite number of hidden layer neurons m and an ideal \mathbf{w}^* , such that the RBF neural network consistently approximates any continuous smooth unknown function \mathbf{d} on a compact set, i.e.:

$$\mathbf{d} = \mathbf{w}^{*T} \boldsymbol{\gamma}(x) + \boldsymbol{\varepsilon}. \quad (25)$$

where $\boldsymbol{\varepsilon} = [\varepsilon_1, \dots, \varepsilon_n]^T$ denotes the approximation error and satisfies $\|\boldsymbol{\varepsilon}(x)\| \leq \bar{\boldsymbol{\varepsilon}}$, $\bar{\boldsymbol{\varepsilon}}$ is a very small real number vector; $\boldsymbol{\gamma}(x) = [\gamma_1(x), \gamma_2(x), \dots, \gamma_m(x)]^T$ is the radial basis function:⁴⁴

$$\gamma_i(x) = \exp\left(-\frac{\|x - c_i\|^2}{\theta_i^2}\right), (i = 1, 2, \dots, q). \quad (26)$$

where $\gamma_i(x)$ is the output of the i th neuron, c_i is the center vector of the Gaussian function of the i th neuron, θ_i denotes the width of the Gaussian basis function of the i th neuron, and q is the number of neurons in the hidden layer of the neural network.

The equivalent disturbance of the RBF neural network output is:

$$\hat{\mathbf{d}} = \hat{\mathbf{w}}^T \boldsymbol{\gamma}(x). \quad (27)$$

where $\hat{\mathbf{d}}$ is the estimated value of the external disturbance; $\hat{\mathbf{w}} = [\hat{w}_1, \hat{w}_2, \dots, \hat{w}_n]^T \in \mathbb{R}^{m \times n}$ is the corresponding neural network weight coefficient matrix.

The disturbance estimation error can be obtained by the (25) and (27):

$$\tilde{\mathbf{d}} = \mathbf{d} - \hat{\mathbf{d}} = (\mathbf{w}^{*T} - \hat{\mathbf{w}}^T) \boldsymbol{\gamma}(x) + \boldsymbol{\varepsilon} = \tilde{\mathbf{w}}^T \boldsymbol{\gamma}(x) + \boldsymbol{\varepsilon}. \quad (28)$$

where $\tilde{\mathbf{w}}$ denotes the fitting error of the weight coefficient matrix between the ideal neural network and the actual neural network. When the error $\tilde{\mathbf{d}} \rightarrow 0$, it means that the output $\hat{\mathbf{d}}$ of the neural network approximates the unknown disturbance \mathbf{d} well.

4 | DESIGN OF APET-MPC CONTROLLER

Traditional MPC is time-triggered, periodic, and only the first control variable is applied to the control system. Event-triggered model predictive control (ET-MPC) executes the task when the event-triggered condition is satisfied, avoiding unnecessary resource waste and achieving a good balance between system performance and resource utilization. The prediction horizon in MPC is usually a fixed constant, that is, each step of solving the optimization problem has the same dimension. We adopt an adaptive method to reduce the prediction range to reduce the dimension and computational complexity of solving the optimization problem.³⁸

Figure 3 shows the structure of APET-MPC control based on the RBF neural network disturbance observer. The high-dimensional linear model of the system obtained by the Koopman operator can be divided into the nominal model without disturbance and the disturbance model considering external disturbance. The APET-MPC controller is designed for the nominal model, and the RBF neural network disturbance observer is designed for the disturbance model to estimate the disturbance of the emergency supplies transportation robot, so that the Koopman high-dimensional model solved offline can better approximate the real system in the actual control process with disturbance, and the emergency supplies transportation robot can accurately track the reference trajectory with fewer triggering times.

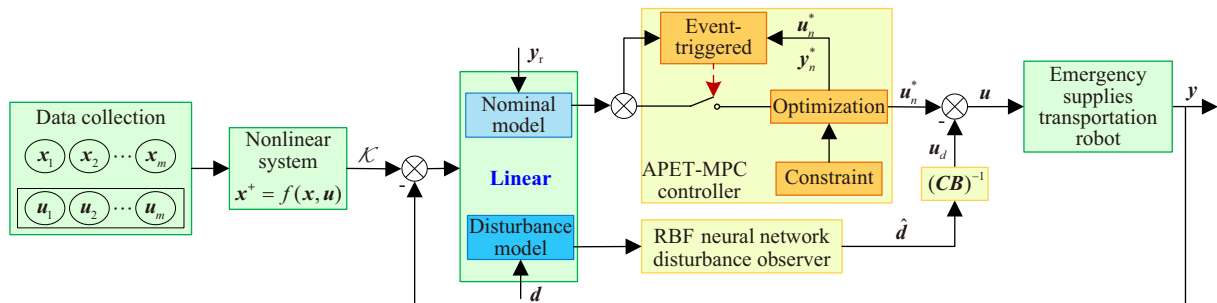


Figure 3 RBF-APET-MPC control structure diagram.

4.1 | Optimization problem

For the Koopman high-dimensional model with disturbance (23), the control output should contain the output of the undisturbed nominal system and disturbance compensation value, and the control variable $\mathbf{u}(k)$ can be expressed as:

$$\mathbf{u}(k) = \mathbf{u}_n(k) - \mathbf{u}_d(k). \quad (29)$$

where $\mathbf{u}_n(k)$ is the nominal system control variable, which can be transformed into linear quadratic programming to solve the problem by MPC. $\mathbf{u}_d(k)$ is the disturbance compensation control variable:

$$\mathbf{u}_d(k) = (\mathbf{CB})^{-1} \hat{\mathbf{d}}(k). \quad (30)$$

The Koopman high-dimensional model corresponding to the nominal system control variable $\mathbf{u}_n(k)$ is:

$$\begin{cases} \mathbf{z}_n(k+1) = \mathbf{A}\mathbf{z}_n(k) + \mathbf{B}\mathbf{u}_n(k) \\ \mathbf{y}_n(k) = \mathbf{C}\mathbf{z}_n(k) \end{cases}. \quad (31)$$

The output expression of the nominal system in the prediction horizon is:

$$\mathbf{y}_n(k+1) = \mathbf{F}\mathbf{z}_n(k) + \mathbf{\Theta}\mathbf{u}_n(k). \quad (32)$$

where,

$$\mathbf{y}_n(k+1) = \begin{bmatrix} \mathbf{y}_n(k+1|k) \\ \mathbf{y}_n(k+2|k) \\ \vdots \\ \mathbf{y}_n(k+N|k) \end{bmatrix}, \mathbf{u}_n(k) = \begin{bmatrix} \mathbf{u}_n(k|k) \\ \mathbf{u}_n(k+1|k) \\ \vdots \\ \mathbf{u}_n(k+N-1|k) \end{bmatrix}, \mathbf{F} = \begin{bmatrix} \mathbf{CA} \\ \mathbf{CA}^2 \\ \vdots \\ \mathbf{CA}^N \end{bmatrix}, \mathbf{\Theta} = \begin{bmatrix} \mathbf{CB} & 0 & \cdots & 0 \\ \mathbf{CAB} & \mathbf{CB} & \cdots & 0 \\ \vdots & \vdots & \ddots & \vdots \\ \mathbf{CA}^{N-1}\mathbf{B} & \mathbf{CA}^{N-2}\mathbf{B} & \cdots & \mathbf{CB} \end{bmatrix}.$$

Define the reference state variable $\mathbf{y}_r(k)$ and the reference control input variable $\mathbf{u}_r(k)$ in the prediction horizon, the error between the actual state and the reference state is $\mathbf{y}_e(k)$, and the control error is $\mathbf{u}_e(k)$.

The objective function is designed to ensure that the emergency supplies transportation robot can track the reference trajectory quickly and smoothly. Design the following objective function:

$$\mathbf{J}(\mathbf{y}_e(k), \mathbf{u}_n(k), N) = \sum_{i=0}^{N-1} \left(\|\mathbf{y}_e(k+i|k)\|_{\mathbf{Q}}^2 + \|\mathbf{u}_e(k+i|k)\|_{\mathbf{R}}^2 \right) + \|\mathbf{y}_e(k+N|k)\|_{\mathbf{P}}^2. \quad (33)$$

where the weight coefficients \mathbf{Q} , \mathbf{R} and \mathbf{P} are diagonal matrices. The first term reflects the accuracy requirement of the system for tracking the reference trajectory of the controller, the second term reflects the stability requirement of the control input,⁴⁵ and the third term is the terminal constraint.

4.2 | Adaptive prediction horizon event-triggered control

In this section, we design the event-triggered mechanism including the triggering condition that determines the triggering time and the update method of the prediction horizon N_{k_j} , so that the optimization problem is solved only at each trigger time. The prediction horizon determines the length of the rolling optimization solution process. When the prediction horizon is long, the stability of the system can be guaranteed, but the computational effort will increase. When the prediction horizon is short, the robustness of the system becomes worse, but the dimension of the optimization problem can be reduced. In the standard MPC, the prediction horizon is a fixed constant, but as the tracking error gradually approaches the terminal region, a shorter prediction horizon is sufficient to satisfy the terminal constraint. Therefore, the adaptive prediction horizon event-triggered mechanism is designed to reduce the computational effort.

Define $\{k_j\}$ as the triggering time series, and the number of adjacent time updates is:

$$k_{j+1} = k_j + T, k_0 = 0. \quad (34)$$

where T is the interval time between events, determined by the current actual state variable. Define N_{k_j} as the prediction horizon of the triggering time k_j , adaptively updated as:³⁸

$$N_{k_{j+1}} = N_{k_j} - L, N_0 = N_p. \quad (35)$$

where L is the length of the prediction horizon shrinkage, which is updated at the current triggering time. N_p is a constant that guarantees the solution of the optimization problem at the initial time. The upper and lower bounds of the event interval time are $\sigma \leq T \leq N_{k_j}$, where σ is an adjustable parameter.

Remark 1. Since the sampling period of the emergency supplies transportation robot system is fixed, and the minimum event interval is σ and the maximum value is N_{k_j} , the system will not exhibit Zeno behavior.

At the triggering time k_j , the optimal state sequence $\mathbf{y}_n^*(k_j)$ and the optimal control sequence $\mathbf{u}_n^*(k_j)$ in the prediction horizon N_{k_j} are obtained by solving the following minimization problem:

$$\begin{aligned} \min_{\mathbf{u}_n(k_j)} \mathbf{J} \left(\mathbf{y}_e(k_j), \mathbf{u}_n(k_j), N_{k_j} \right) \\ \mathbf{y}_e(k_j | k_j) = \mathbf{y}_e(k_j) \\ \text{s.t. } \mathbf{y}_e(k_j + N_{k_j} | k_j) \in \Omega_\varepsilon . \\ \mathbf{u}_n(k_j + i | k_j) \in \mathbb{U} \end{aligned} \quad (36)$$

where $i = 0, \dots, N_{k_j} - 1$, $\Omega_\lambda = \left\{ \mathbf{y}_e : \|\mathbf{y}_e\|_P^2 \leq \lambda^2 \right\}$, and $\lambda > 0$ is the terminal region, the terminal constraint ensures stability by guaranteeing that the state at the end of the prediction horizon enters the terminal set. At each triggering time, the actual state of the robot is obtained by the first constraint to initialize the controller, and the future behavior is predicted by the second control input constraint and the system output (32).

The triggering condition is based on the difference between the actual state variable and the optimal state variable obtained at the previous triggering time, and the Euclidean norm of the difference is defined as $\tilde{\mathbf{y}}(k_j + T | k_j) = \left\| \mathbf{y}_n(k_j + T) - \mathbf{y}_n^*(k_j + T | k_j) \right\|$.

Lemma 1. ⁴⁶The bound of the error is: $\tilde{\mathbf{y}}(k_j + T | k_j) \leq L_f^{T-1} \cdot \tilde{\mathbf{y}}(k_j + T | k_j) + \frac{L_f^{T-1} - 1}{L_f - 1} \cdot \varepsilon \leq \frac{L_f^T - 1}{L_f - 1} \cdot \varepsilon$.

The triggering condition is designed according to Lemma 1:

$$\tilde{\mathbf{y}}(k_j + T | k_j) \geq \frac{L_f^T - 1}{L_f - 1} \cdot \bar{\varepsilon}. \quad (37)$$

where the triggering condition is calculated based on the boundary $\bar{\varepsilon}$ of the disturbance observation error $\tilde{\mathbf{d}}$.

To ensure system stability, the prediction horizon is updated in the form of (35), and the length of the shrinkage is:

$$L = \min \left\{ T - 1, N_{k_j} - \hat{N}_{k_j} \right\}. \quad (38)$$

where $\hat{N}_{k_j} = \inf \left\{ i : \mathbf{y}_e^*(k_j + i | k_j) \in \Omega_\varepsilon \right\}$ is the shortest prediction horizon that guarantees the feasibility of the optimization problem iteration. The prediction horizon at k_{j+1} should satisfy:

$$k_j + N_{k_j} < k_{j+1} + N_{k_{j+1}} \leq k_{j+1} + N_{k_j}. \quad (39)$$

Combined with the triggering condition, MPC solves the optimization problem only in two cases. (i) Each time N_{k_j} is reached. (ii) When the error between the actual state variable and the optimal state variable exceeds $\left(\left(L_f^T - 1 \right) / \left(L_f - 1 \right) \right) \cdot \bar{\varepsilon}$.

Therefore, the triggering rule is:

$$\mathbf{u}_n(k_j + i) = \begin{cases} \mathbf{u}_n^*(k_j + i | k_j), & \text{Triggering condition not valid} \\ \mathbf{u}_n^*(k_{j+1} | k_{j+1}), & \text{Triggering condition valid, solve optimization problem} \end{cases} \quad (40)$$

The event-triggered mechanism can reduce the frequency of optimization problem solving and thereby reducing the computational effort. Algorithm 1 summarizes the event-triggered MPC algorithm with the adaptive prediction horizon.

The first control action of the optimal control sequence $\mathbf{u}_n^*(k_j)$ solved by the optimization problem (36) is the nominal system control variable $\mathbf{u}_n(k_j)$ at time k_j . The final control variable $\mathbf{u}(k)$ of the emergency supplies transportation robot obtained by (29) is:

$$\mathbf{u}(k) = \mathbf{u}_n^*(k_j) - (\mathbf{C}\mathbf{B})^{-1} \hat{\mathbf{d}}(k). \quad (41)$$

Algorithm 1 APET-MPC algorithm

Initialize system information;
while N do not reach the maximum simulation time of the system
 Solve the optimization problem at k_j to obtain the optimal state $\mathbf{y}_n^*(k_j)$ and the optimal control $\mathbf{u}_n^*(k_j)$;
 if **then** $\tilde{\mathbf{y}}(k_j + T|k_j) < \left(L_f^T - 1\right) \cdot \bar{\epsilon} / (L_f - 1)$ or $i < N_{k_j}$
 Apply the control variable $\mathbf{u}_n^*(k_j + i|k_j)$ to the nominal system;
 $i = i + 1$;
 Measure the actual state $\mathbf{y}_n(k_j + i)$ and go to step 4;
 else
 Solve for the event interval time $T = i$;
 Find \hat{N}_{k_j} so that $\mathbf{y}_n^*(k_j + \hat{N}_{k_j}|k_j) \in \Omega_\epsilon$ and $\mathbf{y}_n^*(k_j + \hat{N}_{k_j} - 1|k_j) \notin \Omega_\epsilon$;
 Determine the prediction horizon $N_{k_{j+1}}$ at time k_{j+1} ;
 end if
 Update the triggering time $k_{j+1} \rightarrow k_j$ and go to step 1;
end while

4.3 | Stability analysis

Theorem 1. Set at the time $k_j + i$, the emergency supplies transportation robot is subject to optimal control $\mathbf{u}_n^*(k_j + i|k_j)$, the triggering condition is given by (37), and the length of the prediction horizon shrinkage is given by (38). At this time, the system (31) is stable.

Assumption 4. ⁴⁶The state objective function $\mathcal{S}(\mathbf{y}_e(k + i|k), \mathbf{u}_n(k + i|k))$ is locally Lipschitz continuous and the Lipschitz constant is L_s . Assuming $\mathcal{S}(0, 0) = 0$, then there exist positive integers $a > 0$, $b \geq 1$, and get:

$$\mathcal{S}(\mathbf{y}_e(k + i|k), \mathbf{u}_n(k + i|k)) \geq a \|\mathbf{y}_e(k + i|k), \mathbf{u}_n(k + i|k)\|^b. \quad (42)$$

Assumption 5. ⁴⁶The terminal objective function $\mathbf{H}(\mathbf{y}_e(k + N|k))$ is locally Lipschitz continuous and the Lipschitz constant is L_H . The local state feedback controller $\chi(\mathbf{y}_e(k)) = D\mathbf{y}_e(k)$ exists and satisfies:

$$\mathbf{H}(\mathbf{y}_e(k + N|k + 1)) - \mathbf{H}(\mathbf{y}_e(k + N|k)) \leq -\mathcal{S}(\mathbf{y}_e(k), \chi(\mathbf{y}_e(k))). \quad (43)$$

The optimization problem (33) can be written as:

$$\mathbf{J}(\mathbf{y}_e(k), \mathbf{u}_n(k), N) = \sum_{i=0}^{N-1} \mathcal{S}(\mathbf{y}_e(k + i|k), \mathbf{u}_n(k + i|k)) + \mathbf{H}(\mathbf{y}_e(k + N|k)). \quad (44)$$

Proof. To show the stability of the control system, the core is to prove the monotonic decreasing property of the objective function. The optimization problem is solved at k_j . Define the Lyapunov function as $V(k_j) = \mathbf{J}(\mathbf{y}_e^*(k_j), \mathbf{u}_n^*(k_j), N_{k_j})$, and substitute the optimal solutions at k_{j+1} and k_j into the objective function, that is, the difference between $V(k_{j+1})$ and $V(k_j)$ is:

$$\begin{aligned} \Delta V &= \mathbf{J}(\mathbf{y}_e^*(k_{j+1}), \mathbf{u}_n^*(k_{j+1}), N_{k_{j+1}}) - \mathbf{J}(\mathbf{y}_e^*(k_j), \mathbf{u}_n^*(k_j), N_{k_j}) \\ &= \sum_{i=0}^{N_{k_{j+1}}-1} \mathcal{S}(\mathbf{y}_e^*(k_{j+1} + i|k_{j+1}), \mathbf{u}_n^*(k_{j+1} + i|k_{j+1})) + \mathbf{H}(\mathbf{y}_e^*(k_{j+1} + N_{k_{j+1}}|k_{j+1})) \\ &\quad - \sum_{i=0}^{N_{k_j}-1} \mathcal{S}(\mathbf{y}_e^*(k_j + i|k_j), \mathbf{u}_n^*(k_j + i|k_j)) - \mathbf{H}(\mathbf{y}_e^*(k_j + N_{k_j}|k_j)). \end{aligned} \quad (45)$$

According to the Lipschitz condition, the (45) can be written as:

$$\begin{aligned}
\Delta V = & \sum_{i=0}^{N_{k_j}-1} \mathcal{S} \left(\mathbf{y}_e^*(k_{j+1} + i | k_{j+1}), \mathbf{u}_n^*(k_{j+1} + i | k_{j+1}) \right) - \mathcal{S} \left(\mathbf{y}_e^*(k_{j+1} + i | k_j), \mathbf{u}_n^*(k_{j+1} + i | k_j) \right) \\
& + \mathcal{S} \left(\mathbf{y}_e^*(k_{j+1} + N_{k_{j+1}} | k_{j+1}), \chi \left(\mathbf{y}_e^*(k_j + N_{k_j} | k_{j+1}) \right) \right) - \mathcal{S} \left(\mathbf{y}_e^*(k_j | k_j), \mathbf{u}_n^*(k_j | k_j) \right) \\
& + \mathbf{H} \left(\mathbf{y}_e^*(k_{j+1} + N_{k_{j+1}} | k_{j+1}) \right) - \mathbf{H} \left(\mathbf{y}_e^*(k_j + N_{k_j} | k_j) \right).
\end{aligned} \tag{46}$$

According to Assumption 4, we obtain:

$$\mathcal{S} \left(\mathbf{y}_e^*(k_j | k_j), \mathbf{u}_n^*(k_j | k_j) \right) \geq a \left\| \mathbf{y}_e^*(k_j | k_j), \mathbf{u}_n^*(k_j | k_j) \right\|^b. \tag{47}$$

According to Assumptions 4 and 5, we obtain:

$$\begin{aligned}
\Delta V \leq & L_s \left\| \mathbf{y}_e^*(k_{j+1} + i | k_{j+1}) - \mathbf{y}_e^*(k_{j+1} + i | k_j) \right\| - a \left\| \mathbf{y}_e^*(k_j | k_j) \right\|^b \\
& + \mathbf{H} \left(\mathbf{y}_e^*(k_j + N_{k_j} | k_{j+1}) \right) - \mathbf{H} \left(\mathbf{y}_e^*(k_j + N_{k_j} | k_j) \right) \\
\leq & L_s \frac{\|A\|^{N_{k_j}-1} - 1}{\|A\| - 1} \tilde{\mathbf{y}}(k_{j+1} | k_j) - a \left\| \mathbf{y}_e^*(k_j | k_j) \right\|^b + L_H \|A\|^{N_{k_j}-1} \tilde{\mathbf{y}}(k_{j+1} | k_j).
\end{aligned} \tag{48}$$

From Lemma 1 we obtain:

$$\left(L_s \frac{\|A\|^{N_{k_j}-1} - 1}{\|A\| - 1} + L_H \|A\|^{N_{k_j}-1} \right) \tilde{\mathbf{y}}(k_{j+1} | k_j) < a \left\| \mathbf{y}_e^*(k_j | k_j) \right\|^b. \tag{49}$$

Therefore $\Delta V < 0$, the objective function substituted into the optimal solution must be smaller than the objective function substituted into other feasible solutions. In summary, it can be obtained that the monotonic decreasing property of the objective function holds, that is:

$$\mathbf{J} \left(\mathbf{y}_e^*(k_{j+1}), \mathbf{u}_n^*(k_{j+1}), N_{k_{j+1}} \right) < \mathbf{J} \left(\mathbf{y}_e^*(k_j), \mathbf{u}_n^*(k_j), N_{k_j} \right). \tag{50}$$

Therefore the APET-MPC control system is stable. \square

5 | SIMULATION EXPERIMENTS

In this paper, a joint Carsim/ Simulink simulation model is established to verify the modeling accuracy of Koopman and the performance of the APET-MPC controller based on RBF neural network disturbance observer.

5.1 | Validation of the Koopman model

Since Koopman is a purely data-driven modeling method, the first step is to collect the operational data of the emergency supplies transportation robot. The Koopman linear model shown in (22) is established by using the input-output response characteristics of the robot model provided by Carsim. In the simulation, the sampling period $T_s = 0.02s$ is set and 40 simulations are performed. The initial state of each simulation is set to zero, and a trajectory is obtained every 10s of operation (i.e., each trajectory generates 500 data points), with a total of 20,000 data points. All the collected data are used as the training set to solve the Koopman high-dimensional linear model of the robot. According to the randomly generated robot input-output data as the test set to verify the approximation accuracy of the high-dimensional linear model to the real emergency supplies transportation robot model.

Under the condition of consistent initial state and control input, the simulation compares the accuracy of the model with the traditional local linearization method, Koopman linear model and Carsim model, where the local linearization method is a first-order Taylor expansion at \mathbf{x}_0 . Figure 4 and Figure 5 are the simulation comparison under the robot control input and state dimensions, respectively.

It can be seen from Figures 4 and 5 that the Koopman linear model fits better with the Carsim model, while the local linearization method has some errors. To further demonstrate the superiority of the Koopman linear model, the prediction accuracy of the Koopman model and the local linearization model are compared in different prediction horizons. To quantitatively represent the prediction performance of the model, the normalized root mean square error (NRMSE) shown in (51) is used as a quantitative indicator:

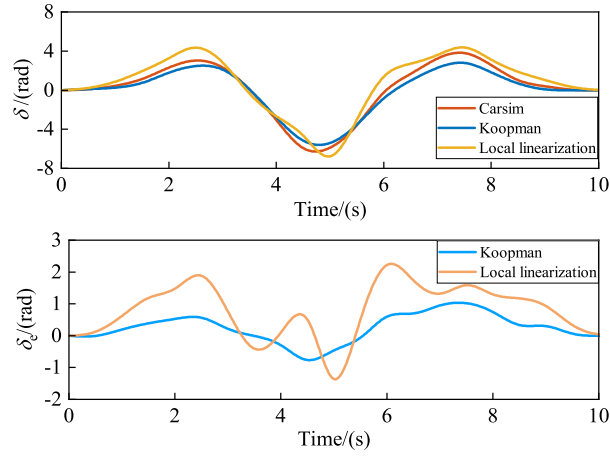


Figure 4 Comparison of control input accuracy.

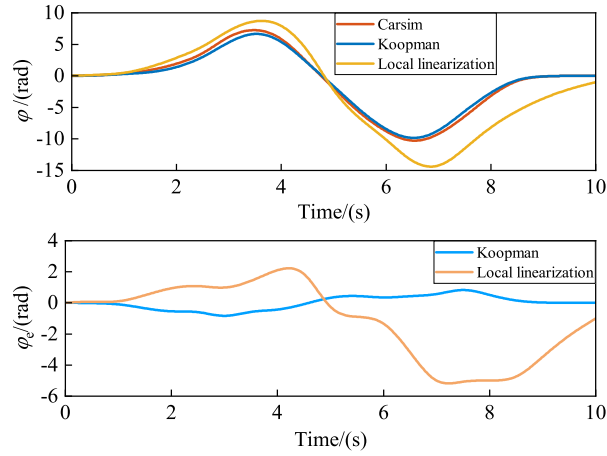


Figure 5 Comparison of state accuracy.

Table 1 NRMSE of yaw angle in the different prediction horizons.

| Prediction horizon | Koopman model | Local linearization model |
|--------------------|---------------|---------------------------|
| 2 | 3.15% | 13.62% |
| 5 | 13.47% | 85.47% |
| 10 | 27.52% | 106.39% |

$$\text{RMSE} = \sqrt{\frac{1}{O} \sum_{k=1}^O (\varphi(k) - \hat{\varphi}(k))^2}. \quad (51a)$$

$$\text{NRMSE} = \frac{\text{RMSE}}{\varphi_{\max}(k) - \varphi_{\min}(k)} \times 100\%. \quad (51b)$$

where φ is the measured yaw angle, $\hat{\varphi}$ is the predicted yaw angle, and O is the size of the test set. Table 1 shows the NRMSE between the real yaw angle and the predicted yaw angle generated by the two robot models in different prediction horizons.

From Table 1, it can be seen that the Koopman linear model has good prediction accuracy in different prediction horizons, while the local linearization model has good prediction result in a short prediction horizon, but the model gradually fails as the prediction horizon increases because it only linearizes at \mathbf{x}_0 . The Koopman operator can capture the global nonlinearity of the robot model, thus avoiding the additional modeling error caused by local linearization. Therefore, the Koopman linear model has high modeling accuracy and can be applied to emergency supplies transportation robot control system.

5.2 | Validation of APET-MPC controller based on RBF neural network disturbance observer

To verify the performance of the designed APET-MPC trajectory tracking controller based on RBF neural network disturbance observer, its disturbance estimation ability and trajectory tracking ability are simulated and verified under different reference trajectories.

The parameter values of the Gaussian basis function are set to $\mathbf{c} = [-0.5 \ 0 \ 0.5]^T$, $\boldsymbol{\theta} = [0.2 \ 0.2 \ 0.2]^T$. The initial position of the robot is (0,0), the sampling time is 0.1s, the simulation time is 30s, the terminal region is $\Omega_\lambda = \{\mathbf{y}_e : \|\mathbf{y}_e\|_P^2 \leq 0.05^2\}$, the minimum prediction step is $\sigma = 4$, and the initial prediction horizon is $N_0 = 20$. The weight coefficients of the objective function are: $Q = \text{diag}(1,1,0.5)$, $R = \text{diag}(0.4,0.4)$, and $P = \text{diag}(0.5,0.5,0.5)$.

5.2.1 | Linear reference trajectory

Given a linear reference trajectory as $y = 5$, the error between the robot and the reference trajectory at the initial time is 5m. To verify the effectiveness of the APET-MPC controller proposed in this paper, the trajectory tracking effect of APET-MPC and the standard MPC is simulated and compared. The trajectory tracking effect under the two control methods is shown in Figure 6, and the state error under the two control methods is shown in Figure 7.

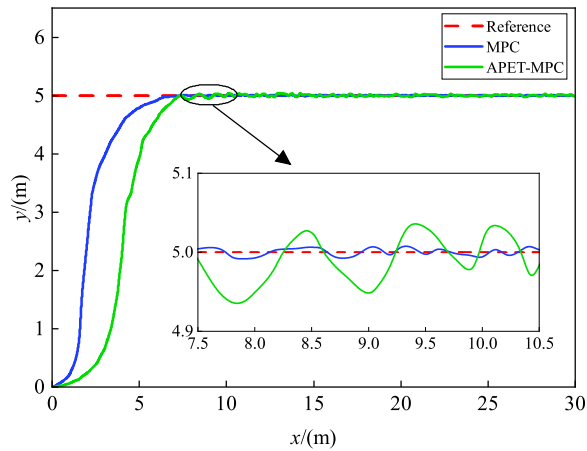


Figure 6 Tracking trajectory of MPC and APET-MPC.

It can be seen from Figure 6 that both MPC and APET-MPC can control the robot to track the reference trajectory, but the tracking curve of MPC is smoother and the tracking effect is better than that of APET-MPC. As can be seen from Figure 7, the state error of the robot eventually converges to 0. Figure 8 shows the triggering time and prediction horizon of standard MPC and APET-MPC. Figure 9 shows the accumulated triggering times for two control methods.

It can be observed from Figure 8 that when the system satisfies the triggering condition, the result is not 0, and the robot triggers events in a finite time, thus avoiding Zeno behavior. The optimization problem (36) of the APET-MPC controller is solved only occur at the triggering time, while the standard MPC is triggered periodically, so it will be triggered at each sampling time. Since APET-MPC adopts the adaptive prediction horizon method when the error between the actual robot state and the reference trajectory decreases, the prediction horizon of the controller also decreases, the dimension of solving the optimization problem also decreases, and the computational complexity of the controller also decreases. In contrast, the prediction horizon of standard MPC is fixed. Under the event-triggered mechanism, the optimization problem is solved when the error between the

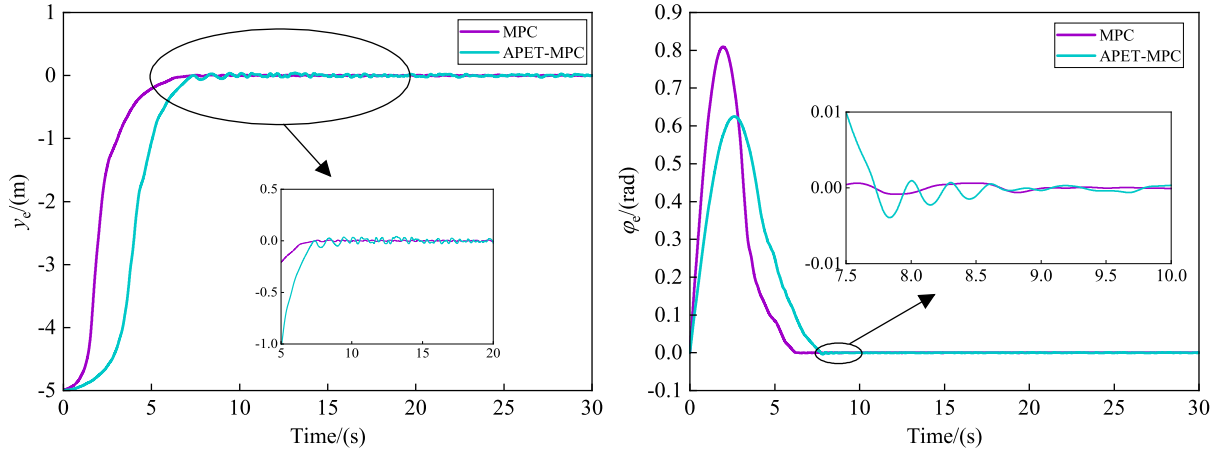


Figure 7 State error of MPC and APET-MPC.

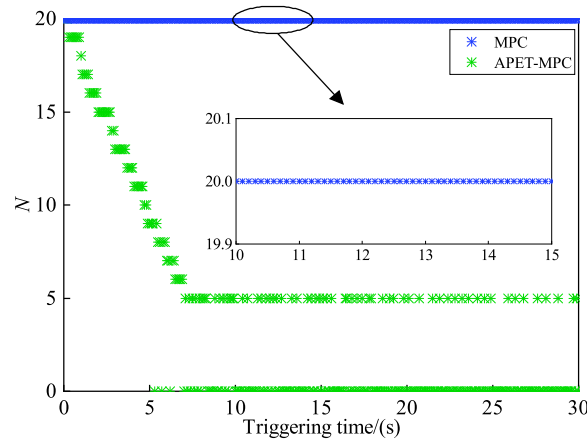


Figure 8 Triggering time and the prediction horizon values of MPC and APET-MPC.

actual trajectory and the optimal trajectory reaches the threshold. According to the prediction horizon update strategy (35), the prediction horizon ultimately decreases to the minimum value of 5. From Figure 9, it can be observed that the triggering times of APET-MPC are significantly reduced compared with the standard MPC, with the accumulated triggering times of the standard MPC being 301 and APET-MPC being 130. Due to the addition of the event-triggered mechanism, the total triggering times of the control system can be reduced by 56.81%. Therefore APET-MPC can reduce the computational complexity compared with standard MPC.

To verify the estimation accuracy of the disturbance by the RBF neural network disturbance observer designed in this paper, a random external disturbance is applied to the robot system at $t = 0s$. The tracking trajectory of the system under the control of MPC, APET-MPC and APET-MPC based on the RBF neural network disturbance observer is given in Figure 10. Figure 11 shows the true value of the disturbance and the estimated value of the RBF neural network disturbance observer to the disturbance.

It can be seen from Figure 10 that the tracking accuracy of MPC and APET-MPC decreases due to disturbance, while the RBF-APET-MPC controller can control the system to stabilize faster. It can be seen from Figure 11 that the RBF neural network disturbance observer can estimate the disturbance to the system effectively. The estimated disturbance value is approximate to the true value with an estimation accuracy is 94.73%, indicating that the designed observer has a good disturbance estimation effect in the stable state. Due to the high accuracy estimation and compensation effect of the neural network disturbance observer, the trajectory tracking effect of the RBF-APET-MPC controller is better than that of the APET-MPC and has better anti-disturbance ability. Compared with MPC relying on its robustness against disturbance, the RBF-APET-MPC controller can achieve real-time disturbance compensation by using the disturbance observer, so it has higher robustness.

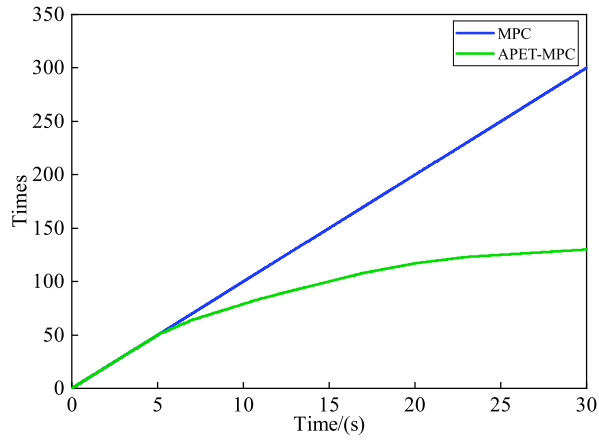


Figure 9 Accumulated triggering times of MPC and APET-MPC.

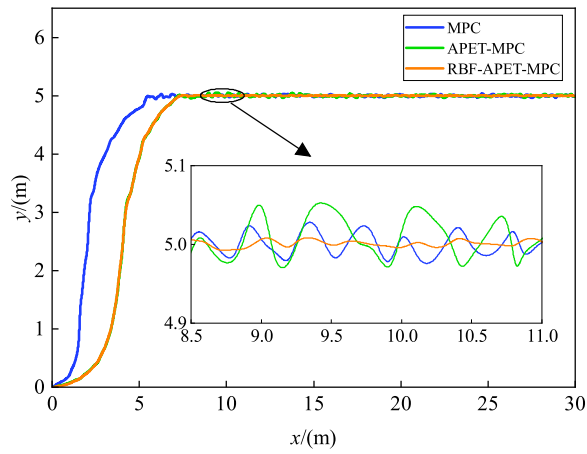


Figure 10 Tracking trajectory under three control methods.

The absolute error integral (IAE) and the time multiplied absolute error integral (ITAE) shown in (52) are selected as evaluation indexes to evaluate the performance of the three controllers.

$$\text{IAE} = \int_0^T |e_x| dt. \quad (52a)$$

$$\text{ITAE} = \int_0^T t |e_x| dt. \quad (52b)$$

where T is the operating time of the system. The IAE and ITAE of the three control methods under the linear reference trajectory are shown in Table 2.

Comprehensive analysis of Figure 9 and Table 2, it can be seen that the triggering times of APET-MPC are reduced, but the IAE and ITAE values are still 1.62% and 12.99% higher than MPC, and the trajectory tracking performance is also reduced. However, the APET-MPC based on RBF neural network disturbance observer has the smallest IAE and ITAE values, especially the ITAE value increases by 82.75%. The results show that APET-MPC based on RBF neural network disturbance observer is superior to the other two control methods in improving the trajectory tracking performance and reducing the computational effort, which verifies the effectiveness and superiority of APET-MPC system based on RBF neural network disturbance observer.

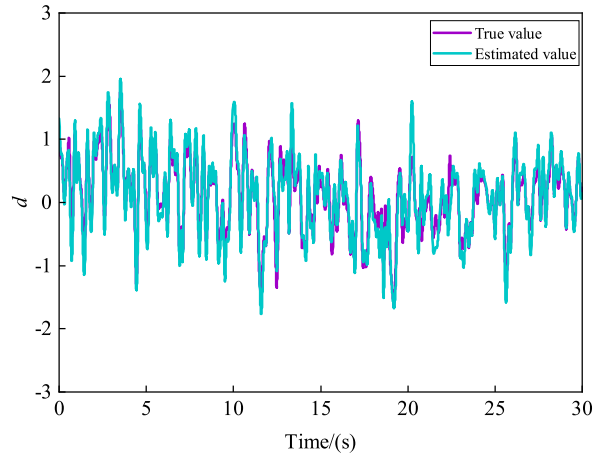


Figure 11 True and estimated values of disturbance.

Table 2 Comparison of trajectory tracking performance of MPC, APET-MPC and RBF-APET-MPC.

| Control method | IAE | ITAE |
|----------------|---------|---------|
| MPC | 20.9313 | 48.1824 |
| APET-MPC | 21.2709 | 54.4401 |
| RBF-APET-MPC | 15.0126 | 8.3118 |

5.2.2 | Double shift reference trajectory

Describe the reference double shift trajectory⁴⁷ by (53):

$$Y_{\text{ref}}(X) = \frac{d_{y1}}{2} (1 + \tanh(z_1)) - \frac{d_{y2}}{2} (1 + \tanh(z_2)). \quad (53a)$$

$$\varphi_{\text{ref}}(X) = \arctan \left(d_{y1} \left(\frac{1}{\cosh(z_1)} \right)^2 \left(\frac{1.2}{d_{x1}} \right) - d_{y2} \left(\frac{1}{\cosh(z_2)} \right)^2 \left(\frac{1.2}{d_{x2}} \right) \right). \quad (53b)$$

where $z_1 = 2.4 \cdot (X - 27.19)/d_{x1} - 1.2$, $z_2 = 2.4 \cdot (X - 56.46)/d_{x2} - 1.2$, $d_{x1} = 25$, $d_{x2} = 21.95$, $d_{y1} = 4.05$, $d_{y2} = 5.7$. The trajectory tracking effect under the standard MPC and APET-MPC control is shown in Figure 12, and the state and control input under the two control methods are shown in Figure 13.

Figure 12 shows both MPC and APET-MPC can control the robot to track the reference trajectory, and the tracking effect of both control methods is approximate. It can be seen from Figure 13 that the control input of the robot under APET-MPC control fluctuates during turning, while the control input of MPC is smoother. Figure 14 shows the triggering time and prediction horizon of standard MPC and APET-MPC.

It can be observed from Figure 14 that the robot does not turn during a period of around 0s to 3.9s, so APET-MPC does not need to solve the optimization problem. There are two points with small turning radii around 4.8s and 13.4s where the actual robot state deviates from the reference trajectory, and the robot needs the control input changes quickly and timely, so the solution of the optimization problem is triggered continuously. This event-triggered mechanism can trigger the solution of the optimization problem at the appropriate time, which reduces the triggering times to solve the optimization problem and saves computational resources. APET-MPC significantly reduces the triggering times compared to standard MPC, with accumulated triggering times of 301 for standard MPC and 138 for APET-MPC. The total triggering times of the control system can be reduced by 54.15%. Therefore, APET-MPC can reduce the computational complexity compared with standard MPC.

To verify the estimation accuracy of the RBF neural network disturbance observer designed in this paper, a random external disturbance is applied to the robot system at $t = 0s$. The tracking trajectory of the emergency supplies transportation robot system under the control of MPC, APET-MPC and APET-MPC based on RBF neural network disturbance observer is given

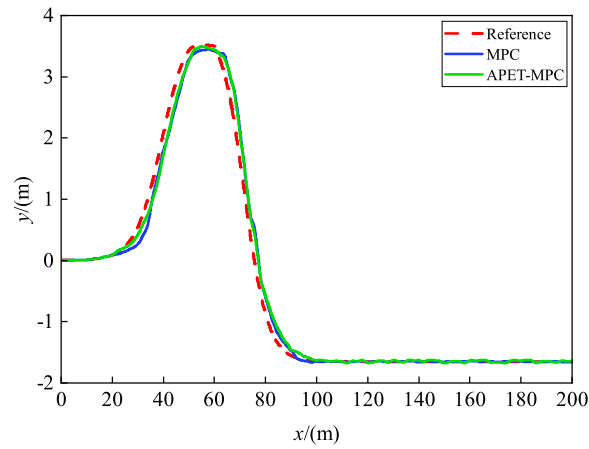


Figure 12 Trajectory tracking of MPC and APET-MPC.

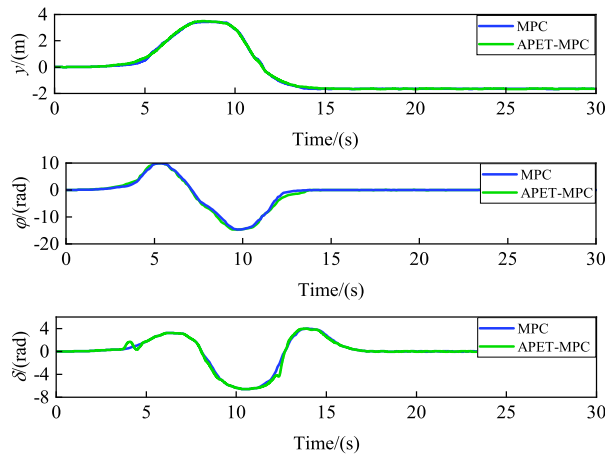


Figure 13 State and control input of MPC and APET-MPC.

in Figure 15. Figure 16 shows the disturbance's true value and the disturbance's estimated value by the RBF neural network disturbance observer.

As can be seen from Figure 15, the tracking accuracy of MPC and ETMPC decreases due to disturbance, while the RBF-APET-MPC controller can maintain good tracking accuracy. From Figure 16, it can be seen that the RBF neural network disturbance observer can estimate the disturbance to the system effectively. The disturbance estimate value is approximate to the true value, and the estimation accuracy is 92.78%, indicating that the designed observer has a good disturbance estimation effect in the stable state. The APET-MPC controller with RBF neural network disturbance observer can use the disturbance observer to achieve real-time control compensation, which has higher stability accuracy compared to MPC.

The IAE and ITAE of the three control methods under the double shift reference trajectory are shown in Table 3.

Based on the comprehensive analysis of Figure 14 and Table 3, it can be seen that APET-MPC has fewer triggering times, but the IAE and ITAE values are still 10.12% and 19.68% higher than MPC, and the trajectory tracking performance has also decreased. However, the APET-MPC based on RBF neural network disturbance observer has the smallest IAE and ITAE values, especially the ITAE value increases by 85.59%. The results show that APET-MPC based on RBF neural network disturbance observer is superior to other methods in improving trajectory tracking performance and reducing computational effort, which verifies the effectiveness and superiority of APET-MPC system based on RBF neural network disturbance observer.

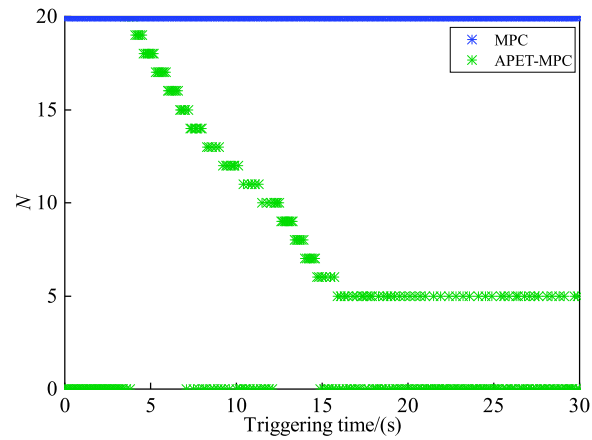


Figure 14 Triggering time and prediction horizon values of MPC and APET-MPC.

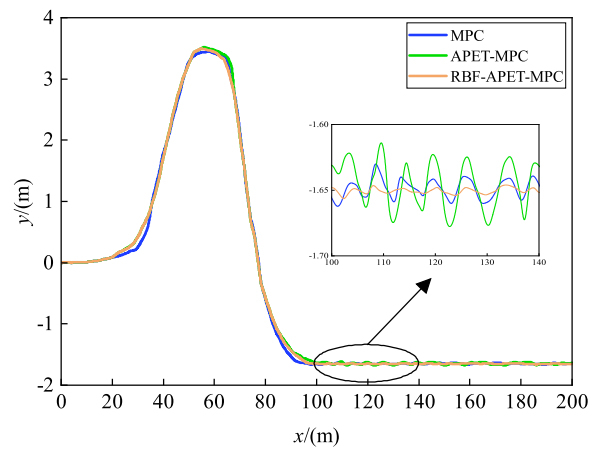


Figure 15 Tracking trajectory under three control methods.

Table 3 Comparison of trajectory tracking performance of MPC, APET-MPC and RBF-APET-MPC.

| Control method | IAE | ITAE |
|----------------|---------|---------|
| MPC | 29.1750 | 47.5305 |
| APET-MPC | 32.1276 | 67.2070 |
| RBF-APET-MPC | 13.1459 | 7.0501 |

6 | CONCLUSIONS

For the trajectory tracking control problem of emergency supplies transportation robot, Koopman operator theory, RBF neural network disturbance observer and APET-MPC method are used to achieve accurate and fast robot tracking of the reference trajectory. The main work includes the following four points:

- (1) The data-driven Koopman operator theory is used in the establishment of the kinematics model. The original control object is transformed from a nonlinear system to a linear system and a high-dimensional linear model of the robot is established,

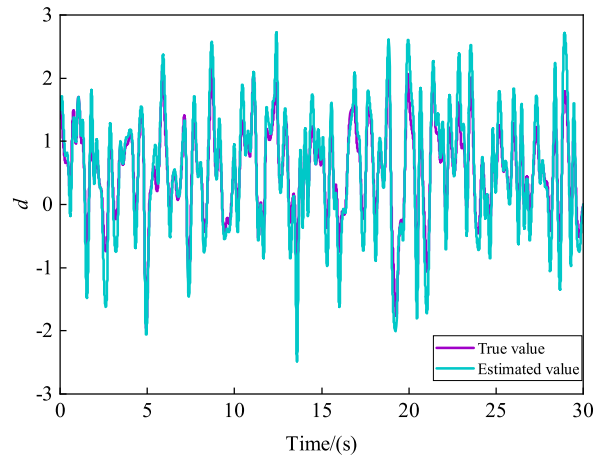


Figure 16 True and estimated values of disturbance.

reducing the difficulty of control law design and computational complexity. At the same time, Koopman is realized by data-driven and only needs to collect operating data from simulation or actual robot, which reduces the requirement for kinematics modeling of emergency supplies transportation robot.

- (2) Considering the complexity of the robot operating environment, the disturbance during operation will have a large impact on the robot trajectory tracking control accuracy, the RBF neural network disturbance observer is designed to estimate the disturbance and compensate it into the controller output, which improves the robustness of the system.
- (3) The APET-MPC method is used to design the controller, which reduces the frequency of solving the optimization problem through the event-triggered mechanism, reduces the dimensionality of the optimization problem by adjusting the prediction horizon and reduces the computational load of the MPC through APET. This reduces the computational load of the controller while ensuring the robot tracking accuracy.
- (4) The joint Carsim/ Simulink simulation model is established to verify the accuracy of the high-dimensional linear model established by the Koopman operator theory and the estimation accuracy of the disturbance by the RBF neural network disturbance observer, and the effectiveness of the APET-MPC controller is simulated under different operating conditions. The experimental results show that the Koopman model can capture the global nonlinearity of robot kinematics, and the prediction error of the Koopman model is smaller than that of the local nonlinear model in different prediction horizons. Compared with the standard MPC, the trajectory tracking error of the APET-MPC trajectory tracking controller is not much different and has better tracking and stability. When there is a disturbance, the RBF neural network disturbance observer can effectively estimate the disturbance with an estimation accuracy above 90%, which can make the robot system quickly track the reference trajectory and reach a stable state, with good anti-disturbance ability.

This work could be extended in the following directions: (i) This paper adopts a purely data-driven method to establish the emergency supplies transportation robot model, but it is difficult to obtain certain data in actual situations, and each collected data is subject to different external disturbance. Future research work will consider how to extract effective data to establish the Koopman model. (ii) The APET-MPC method mentioned in this paper solves the problem of high computational complexity in MPC, which is currently applied to a single robot with relatively small computation complexity. Future research work will consider applying the APET-MPC method to the cooperative control of multiple emergency supplies transportation robots.

ACKNOWLEDGMENTS

This work was financially supported by the National Natural Science Foundation of China under Grant Numbers: 61663021, 71763025 and 61861025.

CONFLICT OF INTEREST

The authors declare that there is no conflict of interest for this article.

References

1. Wang Y, Sun B. Multi-period optimization model of multi type emergency materials allocation based on fuzzy information. *Chinese J of Management Science* 2020; 28(3): 40–51. DOI: 10.16381/j.cnki.issn1003-207x.2020.03.005.
2. Taghizadeh M, Mahsuli M, Poorzahedy H. Probabilistic framework for evaluating the seismic resilience of transportation systems during emergency medical response. *Reliability Engineering & System Safety* 2023; 236: 109255. DOI: 10.1016/j.res.2023.109255.
3. Yu W. A robust model for emergency supplies prepositioning and transportation considering road disruptions. *Operations Research Perspectives* 2023; 10: 100266. DOI: 10.1016/j.orp.2023.100266.
4. Wan M, Ye C, Peng D. Multi-period dynamic multi-objective emergency material distribution model under uncertain demand. *Engineering Applications of Artificial Intelligence* 2023; 117: 105530. DOI: 10.1016/j.engappai.2022.105530.
5. Qin J, Yang K, Xu J, Chen X. Coordination optimization of post-disaster transportation network repair and rescue. *Journal of Railway Science and Engineering* 2022; 19(5): 1206–1214. DOI: 10.19713/j.cnki.43-1423/u.T20210570.
6. Xue X, Wang X, Han T, Ruan J. Study on joint dispatch optimization of emergency materials considering traffic constraints and capacity limits. *Chinese Journal of Management Science* 2020; 28(3): 21–30. DOI: 10.16381/j.cnki.issn1003-207x.2020.03.003.
7. Shen J, Liu K, Ma C, Zhao Y, Shi C. Bibliometric analysis and system review of vehicle routing optimization for emergency material distribution. *Journal of Traffic and Transportation Engineering (English Edition)* 2022; 9(6): 893–911. DOI: 10.1016/j.jtte.2022.10.001.
8. Miranda-Colorado R. Observer-based proportional integral derivative control for trajectory tracking of wheeled mobile robots with kinematic disturbances. *Applied Mathematics and Computation* 2022; 432: 127372. DOI: 10.1016/j.amc.2022.127372.
9. Singhal K, Kumar V, Rana KPS. Robust trajectory tracking control of non-holonomic wheeled mobile robots using an adaptive fractional order parallel fuzzy PID controller. *Journal of the Franklin Institute* 2022; 359(9): 4160–4215. DOI: 10.1016/j.jfranklin.2022.03.043.
10. Adinehvand M, Asadi E, Lai CY, Khayyam H, Hoseinnezhad R. Design and adaptive control of a kinematically redundant robot with enhanced trajectory tracking for climbing in tight spaces. *Mechanism and Machine Theory* 2022; 177: 104994. DOI: 10.1016/j.mechmachtheory.2022.104994.
11. Yin X, Pan L. Enhancing trajectory tracking accuracy for industrial robot with robust adaptive control. *Robotics and Computer-Integrated Manufacturing* 2018; 51: 97–102. DOI: 10.1016/j.rcim.2017.11.007.
12. Sun Z, Hu S, Xie H, Li H, Zheng J, Chen B. Fuzzy adaptive recursive terminal sliding mode control for an agricultural omnidirectional mobile robot. *Computers and Electrical Engineering* 2023; 105: 108529. DOI: 10.1016/j.compeleceng.2022.108529.
13. Matraji I, Al-Durra A, Haryono A, Al-Wahedi K, Abou-Khousa M. Trajectory tracking control of skid-steered mobile robot based on adaptive second order sliding mode control. *Control Engineering Practice* 2018; 72: 167–176. DOI: 10.1016/j.conengprac.2017.11.009.
14. Sun Z, Hu S, He D, Zhu W, Xie H, Zheng J. Trajectory-tracking control of Mecanum-wheeled omnidirectional mobile robots using adaptive integral terminal sliding mode. *Computers and Electrical Engineering* 2021; 96: 107500. DOI: 10.1016/j.compeleceng.2021.107500.

15. Boukens M, Boukabou A, Chadli M. Robust adaptive neural network-based trajectory tracking control approach for non-holonomic electrically driven mobile robots. *Robotics and Autonomous Systems* 2017; 92: 30–40. DOI: 10.1016/j.robot.2017.03.001.
16. Gandarilla I, Montoya-Cháirez J, Santibáñez V, Aguilar-Avelar C, Moreno-Valenzuela J. Trajectory tracking control of a self-balancing robot via adaptive neural networks. *Engineering Science and Technology, an International Journal* 2022; 35: 101259. DOI: 10.1016/j.jestch.2022.101259.
17. Bossi L, Rottenbacher C, Mimmi G, Magni L. Multivariable predictive control for vibrating structures: An application. *Control Engineering Practice* 2011; 19(10): 1087–1098. DOI: 10.1016/j.conengprac.2011.05.003.
18. Cenerini J, Mehrez MW, Han J, Jeon S, Melek W. Model predictive path following control without terminal constraints for holonomic mobile robots. *Control Engineering Practice* 2023; 132: 105406. DOI: 10.1016/j.conengprac.2022.105406.
19. Ding T, Zhang Y, Ma G, Cao Z, Zhao X, Tao B. Trajectory tracking of redundantly actuated mobile robot by MPC velocity control under steering strategy constraint. *Mechatronics* 2022; 84: 102779. DOI: 10.1016/j.mechatronics.2022.102779.
20. Zhao H, Yang H, Wang Z, Li H. Nonlinear switched model predictive control with multiple Lyapunov functions for trajectory tracking and obstacle avoidance of nonholonomic systems. *Int J Robust Nonlinear Control* 2023. DOI: 10.1002/rnc.6690. Accessed March 30, 2023.
21. Yang B, Du W, Wang H. Equivalent Modeling of Virtual Synchronous Generator Based on Data-driven Method. *Power System Technology* 2020; 44(1): 35–43. DOI: 10.13335/j.1000-3673.pst.2019.0245.
22. Peng S, Shi W. Adaptive fuzzy output feedback control of a nonholonomic wheeled mobile robot. *IEEE Access* 2018; 6: 43414–43424. DOI: 10.1109/ACCESS.2018.2862163.
23. Liu X, Wang W, Li X, et al. MPC-based high-speed trajectory tracking for 4WIS robot. *ISA Transactions* 2022; 123: 413–424. DOI: 10.1016/j.isatra.2021.05.018.
24. Mei M, Zhu D, Gan W, Jiang X. The tracking control of unmanned underwater vehicles based on model predictive control. *Control Engineering of China* 2019; 26(10): 1917–1924. DOI: 10.14107/j.cnki.kzgc.151013.
25. Koopman BO. Hamiltonian systems and transformations in Hilbert space. *Proceedings of the National Academy of Sciences of the United States of America* 1931; 17(5): 315–318. DOI: 10.1073/pnas.17.5.315.
26. Bevanda P, Sosnowski S, Hirche S. Koopman operator dynamical models: Learning, analysis and control. *Annual Reviews in Control* 2021; 52: 197–212. DOI: 10.1016/j.arcontrol.2021.09.002.
27. Korda M, Mezić I. Linear predictors for nonlinear dynamical systems: Koopman operator meets model predictive control. *Automatica* 2018; 93: 149–160. DOI: 10.1016/j.automatica.2018.03.046.
28. Ping Z, Yin Z, Li X, Liu Y, Yang T. Deep Koopman model predictive control for enhancing transient stability in power grids. *Int J Robust Nonlinear Control* 2021; 31(6): 1964–1978. DOI: 10.1002/rnc.5043.
29. Son SH, Choi H, Moon J, Kwon JS. Hybrid Koopman model predictive control of nonlinear systems using multiple EDMD models: An application to a batch pulp digester with feed fluctuation. *Control Engineering Practice* 2022; 118: 104956. DOI: 10.1016/j.conengprac.2021.104956.
30. Guo W, Zhao S, Cao H, Yi B, Song X. Koopman operator-based driver-vehicle dynamic model for shared control systems. *Applied Mathematical Modelling* 2023; 114: 423–446. DOI: 10.1016/j.apm.2022.10.014.
31. Li L, Wang T, Xia Y, Zhou N. Trajectory tracking control for wheeled mobile robots based on nonlinear disturbance observer with extended Kalman filter. *Journal of the Franklin Institute* 2020; 357(13): 8491–8507. DOI: 10.1016/j.jfranklin.2020.04.043.
32. Yue X, B L, Liu C, Han H. Neural network disturbance observer-based attitude control for flexible spacecrafts. *Aerospace Shanghai (Chinese & English)* 2023; 39(4): 58–65. DOI: 10.19328/j.cnki.2096-8655.2022.04.006.

33. Sharma M, Kar I. Nonlinear disturbance observer based geometric control of quadrotors. *Asian J Control* 2021; 23(4): 1936–1951. DOI: 10.1002/asjc.2318.
34. He N, Qi L, Li R, Liu Y. Design of a model predictive trajectory tracking controller for mobile robot based on the event-triggering mechanism. *Mathematical Problems in Engineering* 2021; 2021: 1–13. DOI: 10.1155/2021/5573467.
35. Cheng S, Li L, Guo H, Chen Z, Song P. Longitudinal collision avoidance and lateral stability adaptive control system based on MPC of autonomous vehicles. *IEEE Transactions on Intelligent Transportation Systems* 2020; 21(6): 2376–2385. DOI: 10.1109/TITS.2019.2918176.
36. Cai Z, Zhou H, Zhao J, Wu K, Wang Y. Formation control of multiple unmanned aerial vehicles by event-triggered distributed model predictive control. *IEEE Access* 2018; 6: 55614–55627. DOI: 10.1109/ACCESS.2018.2872529.
37. Hung NT, Pascoal AM, Johansen TA. Cooperative path following of constrained autonomous vehicles with model predictive control and event-triggered communications. *Int J Robust Nonlinear Control* 2020; 30(7): 2644–2670. DOI: 10.1002/rnc.4896.
38. Sun Z, Xia Y, Dai L, Campoy P. Tracking of unicycle robots using event-based MPC with adaptive prediction horizon. *IEEE/ASME Transactions on Mechatronics* 2020; 25(2): 739–749. DOI: 10.1109/TMECH.2019.2962099.
39. Pan Z, Liu F. Nonlinear set-membership state estimation based on the Koopman operator. *Int J Robust Nonlinear Control* 2023; 33(4): 2703–2721. DOI: 10.1002/rnc.6536.
40. Williams MO, Kevrekidis IG, Rowley CW. A data-driven approximation of the Koopman operator: Extending dynamic mode decomposition. *J Nonlinear Sci* 2015; 25(6): 1307–1346. DOI: 10.1007/s00332-015-9258-5.
41. Son SH, Narasingam A, Kwon JS. Development of offset-free Koopman Lyapunov-based model predictive control and mathematical analysis for zero steady-state offset condition considering influence of Lyapunov constraints on equilibrium point. *Journal of Process Control* 2022; 118: 26–36. DOI: 10.1016/j.jprocont.2022.08.005.
42. Chen J, Dang Y, Han J. Offset-free model predictive control of a soft manipulator using the Koopman operator. *Mechatronics* 2022; 86: 102871. DOI: 10.1016/j.mechatronics.2022.102871.
43. Hu H, Liu G. H_∞ tracking control of a class of uncertain nonlinear MIMO systems based on neural network disturbance observer. *Control and Decision* 2009; 24(3): 468–471. DOI: 10.13195/j.cd.2009.03.150.huh.029.
44. Huang G. Terminal sliding mode control based on neural network disturbance observer. *Journal of Jilin University (Engineering and Technology Edition)* 2011; 41(6): 726–730. DOI: 10.13229/j.cnki.jdxbgxb2011.06.021.
45. Gao Y, Li R, Shi Y, Xiao L. Design of path planning and tracking control of quadrotor. *Journal of Industrial and Management Optimization* 2022; 18: 2221–2235. DOI: 10.3934/jimo.2021063.
46. Yoo J, Molin A, Jafarian M, Esen H, Dimarogonas DV, Johansson KH. Event-triggered model predictive control with machine learning for compensation of model uncertainties. In: 2017 IEEE 56th Annual Conference on Decision and Control. The organization. ; December 12–15, 2017; Australia. DOI: 10.1109/CDC.2017.8264468.
47. Zhang H, Zhang H, Wang Z, Huang C, Li Y. Adaptive event based predictive lateral following control for unmanned ground vehicle system. *Int J Robust Nonlinear Control* 2021; 31(10): 4744–4763. DOI: 10.1002/rnc.5535.

How to cite this article: Zhang Y., Tang M., Zhang H., Yan Y. An B. Wang W., Tang K.. Emergency supplies transportation robot trajectory tracking control based on Koopman and improved event-triggered model predictive control, *Int J Robust Nonlinear Control*, 202X;XX:X–X.